The influence of cooling rate on the microstructure of an Al–Ni hypereutectic alloy

G. Gonzalez[a,*], G.A. Lara-Rodriguez[a], A. Sandoval-Jiménez[b], W. Saikaly[c], A. Charai[c]

[a]Instituto de Investigaciones en Materiales, Universidad Nacional Autónoma de México, Ciudad Universitaria, A.P. 70-360, 04510 México D.F., Mexico
[b]Instituto Nacional de Investigaciones Nucleares, A.P. 18-102; ESIME UC, IPN, México D.F., Mexico
[c]Laboratoire CP2M / TECSEN, UMR 6122, C.N.R.S. Faculté des Sciences et Techniques de St. Jérôme F-13397 MARSEILLE Cédex 20, France

ARTICLE DATA

Article history:
Received 1 March 2006
Received in revised form
26 November 2007
Accepted 26 February 2008

Keywords:
Melt spinning
Aluminum alloys
Nickel aluminides

ABSTRACT

An Al–4 at.% Ni alloy was prepared by a melt spinning technique and characterized by X-ray diffraction, scanning electron microscopy, energy dispersive X-ray spectroscopy and high resolution transmission electron microscopy. The resulting ribbon microstructure consists of intermetallic Al_9Ni_2 globular-like structures embedded within an aluminum matrix. Characteristic globules are nanometric (~100 nm) and are mainly located at the grain boundaries. The resulting effect on the mechanical properties is the enhancement of the alloy hardness from 58 to 371 HV.

1. Introduction

Most aluminum-based alloys show poor mechanical resistance compared to other metallic-based alloys. Nevertheless, because of their low density, these alloys are very attractive for a large number of applications. One of the methods for enhancing the mechanical properties of these alloys is the addition of a second phase with a high elastic modulus. The resulting alloy is a composite in which the new properties can be evaluated by the rule of mixtures. Within this context, this study examines the reinforcement of the aluminum matrix with dispersed intermetallic Al–Ni particles. Previous results indicated an enhancement of wear resistance when nickel aluminide is present in Al alloys [1]. Intermetallic compounds based on the Al–Ni system are characterized by low density, high strength, good oxidation resistance and, for some of them, an improvement in strength with increasing temperature [2]. However, the drawback of these intermetallics is their low ductility at low temperature.

The constitution of binary alloys of aluminum with nickel is well known; It consists of two solid solutions, (Al) and (Ni), and the intermetallic phases $AlNi_3$, AlNi, Al_3Ni_2, Al_3Ni and Al_3Ni_5. Further thermodynamic information within the Al–Ni system is available in other published work [3].

Among all the metastable phases within the Al–Ni system, the richest in aluminium is Al_9Ni_2. It was first reported by Li and Kuo [4], who claimed that it is isostructural with Al_9Co_2. In more recent studies, Pohla and Ryder argue that the two phases are closely related but not identical [5]. These authors report the lattice parameters of Al_9Ni_2 from X-ray diffraction of samples which exhibited many other phases besides Al_9Ni_2. Unfortunately, there are no reports about either the crystallographic data of Al_9Ni_2, or the XRD spectrum detailing the (*hkl*) planes associated to this

* *Corresponding author.*
E-mail address: joseggr@servidor.unam.mx (G. Gonzalez).

1044-5803/$ – see front matter © 2008 Elsevier Inc. All rights reserved.
doi:10.1016/j.matchar.2008.02.006

phase. Experimental conditions to produce this compound are also ignored.

It is well known that good control of the intermetallic phase microstructure is necessary to attain alloys with adequate ductility [6]. Al–Ni cast products are brittle and inadequate for structural applications. Research is therefore focused on obtaining a microstructure with improved properties.

The aim of this work is to examine the morphology of the intermetallic phase under different rapid solidification conditions. Our objective is to transform the as-cast Al_3Ni needle morphology into a globular Al_9Ni_2 well-dispersed phase. We think that this can be achieved by rapid solidification methods. It is well known that such a process can result in the formation of new metastable phases, and it is a convenient way of producing supersaturated solid solution phases [7,8].

In this study, we correlate the microstructure of the intermetallic Al_9Ni_2 phase with cooling rate. Cooling rate is controlled by the angular speed of the copper wheel used in the chill block melt spinning casting technique. The resulting microstructures are observed and analyzed by electron microscopy and energy dispersive spectroscopy (EDS). Finally, the effect of the microstructure on the mechanical properties was evaluated by microindentation hardness tests.

2. Experimental Procedures

An ingot of an Al–4 at.% Ni alloy, henceforth referred to as Al–4Ni, was prepared in an induction furnace under helium atmosphere in a graphite crucible. Commercial grade elements Al-99.5% and Ni-99% were used as starting materials.

The ingot was melted in a quartz tube and ejected through a nozzle on to the surface of a spinning, copper wheel (200 mm in diameter). The size of the circular nozzle was 1 mm in diameter. Experiments were made under a helium atmosphere in order to avoid melt oxidation. The resulting melt spun ribbons were 25–36 μm thick and 3 mm wide.

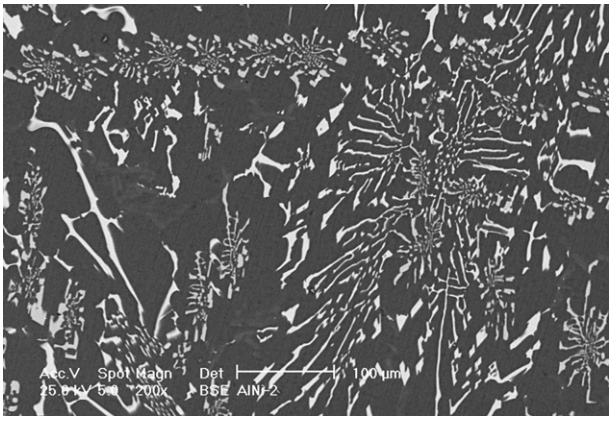

Fig. 1 – SEM image showing the microstructure of the of the Al–4Ni induction as-cast alloy. There are some Al_3Ni needles embedded in the Al rich matrix. From elemental composition by EDS, the white zones composition correspond to Al–6.4 at.% Ni, and the dark zones correspond to Al.

Fig. 2 – SEM micrograph showing intermetallic globules embedded in an Al rich matrix. The alloy sample was melt spun at 21 m/s.

The chamber of the melt spinning device was purged with helium several times before melting. The temperature of the melts was measured by a two-color infrared pyrometer. The velocity of the wheel was determined by a digital tachometer. Three velocities were selected for this study: 21, 37 and 52 m/s. Although the wheel speed is not the only factor determining the cooling rate, monitoring the parameter through wheel speed is qualitatively feasible.

Microstructural characterization was performed by scanning electron microscopy equipped with an EDS analysis system. The ribbons were observed for both in-plane and cross section views. High resolution images were obtain using a JEOL 2010F electron microscope, equipped with a field emission gun and with a spatial resolution of 0.19 nm. Most samples used for high resolution transmission electron microscope (HRTEM) were as-cast ribbon samples. When necessary, the samples were thinned by standard methods

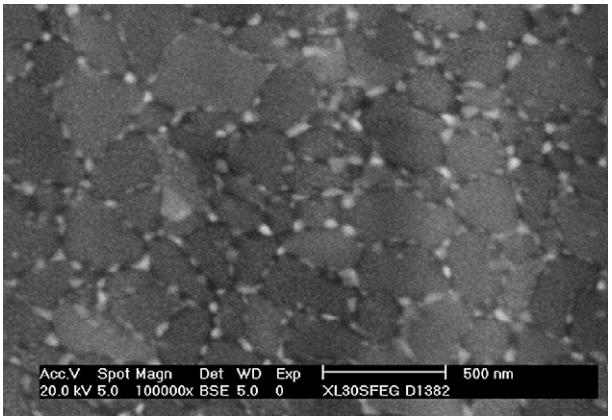

Fig. 3 – SEM microstructure showing intermetallic globules embedded into grain boundaries. The alloy sample was melt spun at 52 m/s.

Table 1 – Standardless EDS element compositions from cross section views

Speed (m/s)	Zone	at.% Al	at.% Ni	Remarks
21	fs	97.50	2.50	Ni gradient towards contact
21	1	96.90	3.10	surface.
21	2	96.01	3.99	
21	cs	95.00	5.00	
37	fs	97.42	2.58	Ni gradient towards contact
37	1	97.28	2.72	surface.
37	2	97.17	2.83	
37	cs	97.02	2.98	
52	fs	97.45	2.55	Very thin sample, no intermediate
52	cs	97.31	2.69	points, same Ni gradient.

fs = free surface, 1,2, intermediate points, cs = contact surface.

(mechanical dimpling and ion milling procedure) in order to determine representative features of the sample. X-ray measurements were made with a D8 Advance Brucker diffractometer with a monocromated Cu Kα radiation. Micro-indentation hardness measurements were carried out using standard equipment, with a load of 50 g for 10 s. (It is worth noting that in melt spun ribbons, the hardness may become load dependent if the applied load exceeds a critical value [9]).

3. Results and Discussion

According to the Al–Ni phase diagram for a nominal composition of Al–4Ni, we expect to form the stoichiometric compound Al_3Ni embedded into an Al rich matrix. Fig. 1 is an SEM backscattered electron image (BSI) micrograph of the induction cast alloy. It shows needles of Al_3Ni (white phase) dispersed into the matrix. This morphology is responsible for the brittle behavior of the alloy.

In contrast, under rapid solidification conditions, the melt spun ribbons show inter-granular particles that have a globular morphology, as shown in Figs. 2 and 3.

As the particles were too small for identification by EDS spectra, only structural aspects determined from XRD analysis and HREM images were employed to characterize these globules. Al_9Ni_2 and small quantities of Al_3Ni were then identified by their diffraction peaks and by HREM direct image and its associated Fast Fourier Transform.

Depending on the wheel speed, the globules are distributed mainly on the grain boundaries. This behavior can be explained as follows:

Upon rapid solidification, the intermetallic Al_9Ni_2 phase starts to precipitate at zones that are richer in Ni concentration. Very soon afterwards, aluminum starts to solidify pushing ahead Ni and thereby enriching the liquid phase in this element. When the Ni concentration in this liquid reaches the saturation level (grain boundaries for example) precipitation of other intermetallic phase occurs. Depending on the level of Ni concentration there are two possible phases; Al_9Ni_2 and Al_3Ni. For higher wheel speeds, the same mechanism takes place except for the differences in the number of nucleation sites and the diffusion rate of Ni which leads to a finer intra-granular and inter-granular intermetallic phase.

The cross section EDS analysis revealed different compositions depending on the distance from the contact surface of the ribbon with the wheel. The contact surface is suppose to be

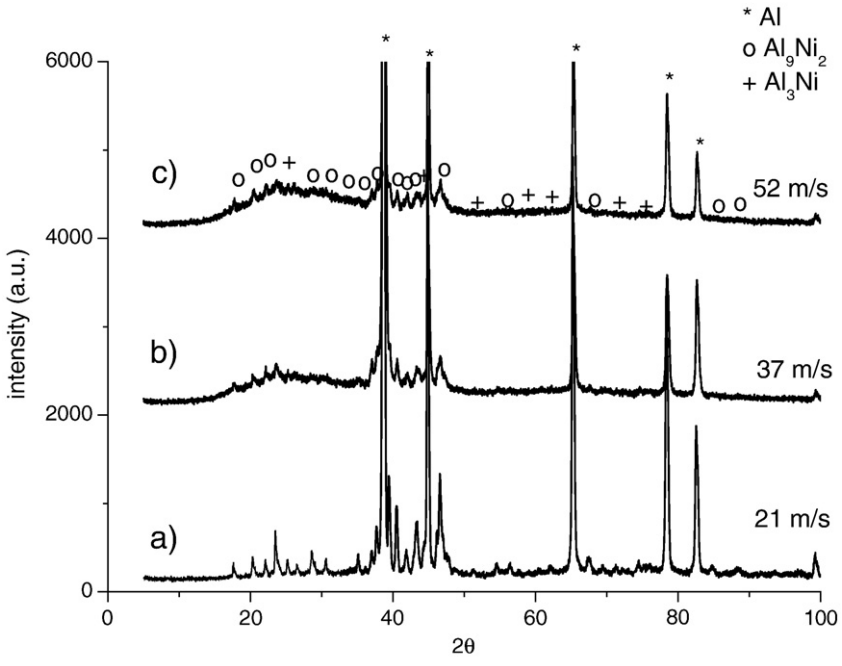

Fig. 4 – XRD diffraction patterns for ribbon samples obtained at different wheel speeds a) 21 m/s, b) 37 m/s, c) 52 m/s.

the zone where the intermetallic phase first solidifies and where there is a greater concentration of nickel and lower content of aluminum (Table 1).

The EDS results point to the increase of Ni solubility in the matrix with increasing cooling rate (because the counting of the Al_9Ni_2 phase was near to its nominal composition). It should be mentioned that some compositional nanoscale inhomogeneities have been reported in similar melt spun Ni-rich alloys [10], but such features are too small to be detected by this technique.

The XRD diffractogram shown in Fig. 4 exhibits several peaks, associated to Al_9Ni_2 phase together with aluminum matrix. The Al_9Ni_2 phase is reported as part of the aluminum-rich side within the binary Al–Ni diagram under non-equilibrium, rapid solidification conditions, and it appears to be always accompanied by several intermetallic compounds [5]. In our case, we obtain this phase with a small amount of Al_3Ni and the aluminum matrix (Fig. 4). The lattice parameters and the Miller indices are shown in Table 2. Note the good fit between experimental and calculated peak positions, with the exceptions of (201) and (401) planes, which do not obey the extinction rule ($0hl$; $l=2n$)

Table 2 – Measured an fitted X-ray diffraction lines of Al_9Ni_2 phase

hkl	d exp (A)	2θ exp	2θ calc	$\Delta 2\theta$	Intensity
(1 1 0)	5.0381	17.589	17.587	0.002	24
(0 1 1)	4.3721	20.295	20.293	0.002	29
(1 1 1)	3.7844	23.489	23.484	0.005	49
(2 1 0)	3.5338	25.181	25.172	0.009	27
(2 0 1)	3.3573	26.528	26.5	0.028	22
(0 2 0)	3.1184	28.602	28.678	−0.076	35
(1 2 0)	2.9242	30.546	30.542	0.004	27
(−2 0 2)	2.6382	33.953	34.022	−0.069	20
(1 1 2)	2.5548	35.097	35.086	0.011	31
(−3 1 1)	2.4857	36.106	36.166	−0.060	20
(−2 1 2)	2.4291	36.977	37.046	−0.069	35
(2 0 2)	2.3846	37.693	37.686	0.007	53
(2 2 1)	2.2831	39.435	39.442	−0.007	98
(2 1 2)	2.226	40.492	40.474	0.018	73
(−1 2 2)	2.1569	41.847	41.84	0.007	35
(3 2 0)	2.1041	42.95	42.89	0.060	33
(−3 1 2)	2.0871	43.318	43.352	−0.034	58
(4 0 1)	1.9654	46.149	46.157	−0.008	49
(3 2 1)	1.9479	46.589	46.59	−0.001	100
(1 3 1)	1.9034	47.744	47.792	−0.048	29
(4 1 1)	1.8744	48.531	48.546	−0.015	20
(−4 2 1)	1.7379	52.621	52.593	0.028	15
(4 0 2)	1.6814	54.533	54.567	−0.034	24
(−5 2 1)	1.4932	62.11	62.129	−0.019	22
(0 4 2)	1.3873	67.458	67.437	0.021	29
(−6 0 2)	1.3527	69.425	69.396	0.029	20
(−6 1 2)	1.3221	71.271	71.262	0.009	22
(−3 4 2)	1.2726	74.502	74.507	−0.005	24
(−4 3 3)	1.2498	76.101	76.092	0.009	22
(0 2 5)	1.1433	84.718	84.705	0.013	22
(−6 0 4)	1.1069	88.204	88.208	−0.004	20
(−4 4 3)	1.1037	88.52	88.528	−0.008	20
(−7 3 1)	1.057	93.57	93.57	0.000	20
(0 0 6)	1.0246	97.496	97.496	0.000	16

Lattice parameters are compatible with a monoclinic cell $a=8.6393$ A, $b=6.2206$ A, $c=6.1811$ A and $\beta=95.98°$

established by the Al_9Co_2 space group (14) $P2_1/c$. Although there are no reports about the Al_9Ni_2 space group, we think that Al_9Ni_2 and Al_9Co_2 are closely related phases, even if they are not iso-structural (same space group). Among the possible monoclinic space groups that permit the existence of (201) and (401) planes with similar symmetry, we can mention the space group (4) $P2_1$, where the condition limiting possible reflections is ($0k0$); $k=2n$.

From Fig. 4, the peaks belonging to the equilibrium phase Al_3Ni seem to vanish for samples at 37 m/s and 52 m/s. On the contrary, the non-equilibrium phase Al_9Ni_2 is present for all tested speeds. Nevertheless, it is difficult to quantify the relative amount of Al_9Ni_2 and Al_3Ni and their evolution as a function of time, due to the low intensity of their XRD peaks and the amorphous broadening affecting the spectra at higher wheel speeds.

Fig. 5 shows TEM images exhibiting the morphology of the Al_9Ni_2 phase. The electron diffraction patterns confirm the presence of Al_9Ni_2 crystals.

HRTEM images in Fig. 6 revealed the presence of Al_9Ni_2 phase in the form of small crystalline aggregates of ~5 nm. The Fast Fourier Transform (FFT) from this picture show a pattern indexed along [010] zone axis. This orientation allows direct measurement of the beta angle of the monoclinic cell (95.9°); this result differs slightly from that reported by Li and Kuo, and Pohla [5,6] who estimated $\beta=96.50°$ by means of X-ray diffraction of a polycrystalline sample. This present angle determination and the lattice parameters fit very well with the X-ray cell refinement, which results in a monoclinic cell with $a=8.6393$ A, $b=6.2206$ A, $c=6.1811$ A and $\beta=95.98°$.

The microindentation hardness measurements of ribbon samples. The data show improvements made to the microstructure by rapid solidification are given in Table 3. For alloys melt spun at 21 and 37 m/s, the hardness values were 200 and 370 HV respectively. These HV values represent an increase of more than 150% compared to the induction as-cast alloy (58 HV). This improvement can be explained in terms of the increase in the dislocation density and the distribution and morphology of the intermetallic phase Al_9Ni_2.

Additional work is currently in progress to ascertain the mechanical properties of these alloy ribbons by other testing methods.

4. Conclusions

The present work investigated the influence of cooling rate (wheel speed) on the microstructure of Al–Ni ribbons. The different intermetallic compounds that formed under rapid solidification were identified and characterized. The conclusions may be summarized as follows.

- The rapid solidification of the Al–4Ni alloy by melt spinning resulted in the formation of globular-like Al_9Ni_2 and Al_3Ni intermetallic phases interspersed in an aluminum-rich matrix. The structural characterization of the Al_9Ni_2 phase led to some corrections in the monoclinic cell parameters compared with earlier literature reports.

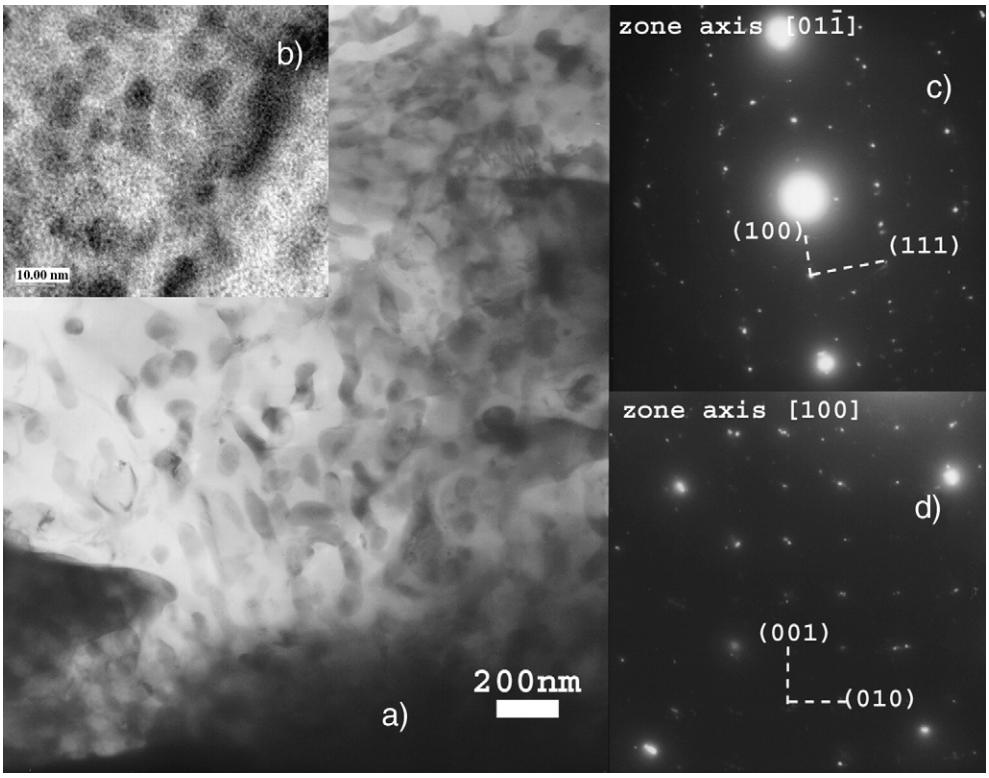

Fig. 5 – a) TEM image showing the morphology of the Al_9Ni_2 phase. b) A magnified view of the same region, c–d) electron diffraction pattern of two Al_9Ni_2 crystals.

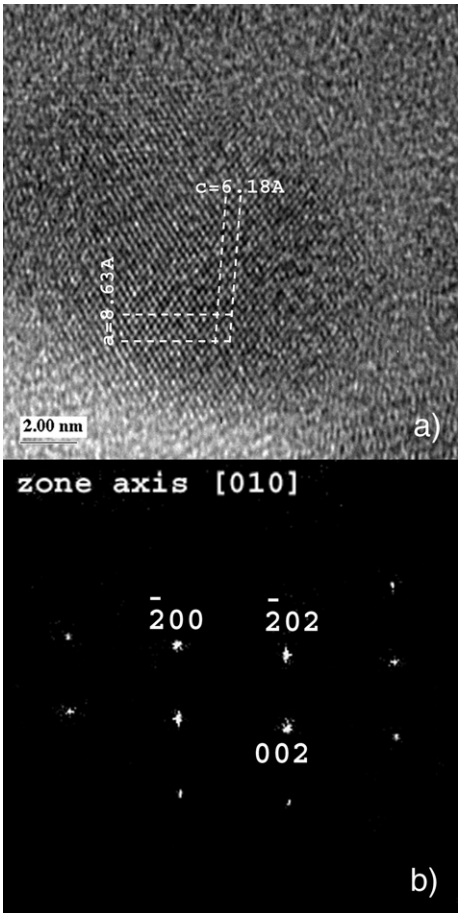

Fig. 6 – a) HRTEM image showing a crystal of Al_9Ni_2 with [010] zone axis, b) FFT image of the same crystal.

- Morphology and distribution of intermetallic particles changed with cooling rate. The concentration of these particles at grain boundaries and higher cooling rates, formed a microstructure that retained a high dislocation density. These phenomena could explain the increase of (Vickers) hardness observed.
- It is possible to assert that the Al_9Ni_2 intermetallic peaks correspond to a slightly distorted cell close to the Al_9Co_2 phase reported in JCPDS card, but with a different space group, according to the extinction rules.

Acknowledgments

The authors are grateful to L. Baños and C. Flores for technical assistance. Financial support is also acknowledged from project IX112204 PAPIIT-UNAM.

Table 3 – Vickers hardness as a function of wheel speed

Sample	Vickers hardness
As cast	58±7
21 m/s	200±13
37 m/s	370±14
52 m/s	Too brittle to be measured

REFERENCES

[1] Da Costa CE, Zapata WC, Velazco F, Ruiz Prieto JM, Torralba JM. Wear behaviour of aluminum reinforced with nickel aluminide. J Mater Process Technol 1999;92–93:66–70.

[2] Ghomashchi MR. Fabrication of near net-shaped Al-based intermetallics matrix composites. J Mater Process Technol 2001;112:227–35.

[3] Chrifi-Alaoui FZ, Nassik M, Mahdouk K, Gachon JC. Enthalpies of formation of the Al–Ni intermetallic compounds. J Alloys Compd 2004;364(Issues 1–2):121–6.

[4] Li XZ, Kuo KH. The decagonal quasicrystals with different periodicity. Philos Mag Lett 1988;58:167–71.

[5] Pohla C, Ryder PL. Crystalline and quasicrystalline phases in rapidly solidified Al–Ni alloys. Acta Mater 1997;45(No 5):2155–66.

[6] Kumar KS. Ternary intermetallics in aluminium-refractory metal-x systems (x = V, Cr, Mn, Fe, Co, Ni, Cu, Zn). Int Mater Rev 1990;35–6:293–327.

[7] Gogebakan M, Uzun O, Karaaslan T, Keskin M. Rapidly solidified Al–6.5 wt% Ni alloys. J Mater Process Technol 2003;142:87–92.

[8] Lavernia EJ, Ayers JD, Srivatsan TS. Rapid solidification processing with specific application to aluminium alloys. Int Mater Rev 1992;137(No1):1–43.

[9] Uzun O, Karaaslan T, Keskin M. Hardness evaluation of Al–12Si–0.5Sb melt-spun ribbons. J Alloys Compd 2003;358:104–11.

[10] Potapov PL, Ochin P, Pons J, Schryvers. Nanoscale inhomogeneities in melt-spun Ni–Al. Acta Mater 2000;48:3833–45.